Surface ordering in a concentrated suspension of colloidal particles investigated by x-ray scattering methods

Anders Madsen,* Oleg Konovalov, Aymeric Robert, and Gerhard Grübel

European Synchrotron Radiation Facility, Boîte Postale 220, 38043 Grenoble, France

The spatial arrangement of colloids near the free surface of a concentrated suspension of colloidal silica in water is investigated by means of x-ray scattering. The weakly charged particles are found to organize in layers along the surface normal direction. The degree of layering decreases with increasing distance from the surface and three layers are identified from the scattering profile. In the lateral direction, the scattering profile indicates a random spatial arrangement of particles at the surface. Based on the findings, a simple structural model for the near surface arrangement of colloidal particles in this system is proposed.

I. INTRODUCTION

The organization of colloidal particles near the liquid/vapor interface has been a subject of major interest in recent years. The abrupt liquid/vapor interface has interesting consequences for the behavior of colloids trapped in this region, and the formation of a variety of structures has been observed in both, experiments and computer simulations. This ranges from the formation of two-dimensional (2D) colloidal crystals with long-range order [1–6] to different types of aggregates [7], including the formation of so-called mesostructures in colloidal monolayers [8]. While the lateral organization of particles at the surface has been studied, we are not aware of any thorough examination of the near-surface organization of colloidal particles including an eventual organization along the surface normal direction. In this experiment, we use x-ray scattering to obtain information on both the lateral and vertical particle organization near the free surface of a suspension of colloidal silica in water. Specular x-ray reflectivity (XR) measurements were used to probe the electron-density profile along the surface normal direction (z direction). Modeling of the measured reflectivity profile then gives information about the organization and layering along the z direction. Lateral organization near the surface may be studied by grazing incidence small-angle x-ray scattering (GISAXS) by varying the momentum transfer q_y in the lateral plane. Here, the grazing incidence of the beam ensures us that only the near surface region is probed. Information about both the size and shape of the particles was obtained by small-angle x-ray scattering (SAXS) from a bulk sample.

Our main result is the observation of particle layering along the surface normal direction in a concentrated colloidal suspension. The degree of the layering decreases with increasing distance from the surface, while the spatial arrangement within the layers is random. The article is organized as follows: In Sec. II, we describe the experimental details. In Sec. III, we present and illustrate the experimental results obtained by using x-ray reflectivity (Sec. III A), small-angle x-ray scattering (Sec. III B), and grazing incidence small-angle scattering (Sec. III C). The findings are summarized and discussed in Sec. IV.

II. EXPERIMENTAL DETAILS

The sample was a suspension of colloidal silica (diameter ~ 320 Å) in water [9] with a weight concentration of 40%. During the experiments, the sample was either contained in thin 0.3 mm quartz capillaries or in a large, flat trough. All experiments were carried out at room temperature. The x-ray measurements were performed at the Troïka Beamlines at the European Synchrotron Radiation Facility. SAXS data were taken at ID10A with x rays of 8 keV ($\lambda = 1.55$ Å) energy provided by a single bounce Si(111) monochromator in Bragg geometry. A Pt-coated mirror was used to suppress higher-order x rays. The monochromatic beam was collimated to a size of 100×100 μm^2 before impinging on the sample capillary situated in an evacuated SAXS chamber. The incident flux was $\sim 1 \times 10^{11}$ photons/sec. The scattered intensity was recorded with a scintillation detector located 2330 mm downstream from the sample. A pair of slits in front of the detector were used to define the scattering angle 2θ and the momentum transfer $q = (4\pi/\lambda)\sin\theta$.

The GISAXS and XR studies were carried out using the liquid scattering diffractometer at ID10B. Two diamond (111) crystals in Bragg geometry were used to select a 8 keV beam that subsequently was reflected from two Pd-coated silicate glass mirrors in order to suppress higher-order x rays. The experiment employed a "liquid reflectivity geometry" in which the angle between the surface and the incident and outgoing beams, θ_i and θ_o, respectively, may be varied continuously without tilting the sample [10]. This requires a deflecting device in front of the sample, and here, a Ge(111) Bragg deflector was used. The corresponding scattering geometry is sketched in Fig. 1. The sample was contained on a polished 100 mm diameter Si wafer by a Teflon barrier. The sample had a large meniscus so that the surface was not shadowed by the barrier and a large footprint could be accepted. A closed outer cell allowed us to stabilize the sample at room temperature and a constant flow of helium into the cell minimized parasitic air scattering. Two large Kapton windows at both the entrance and exit side allowed maximum δ- and θ angles of 20° and 10°, respectively. The

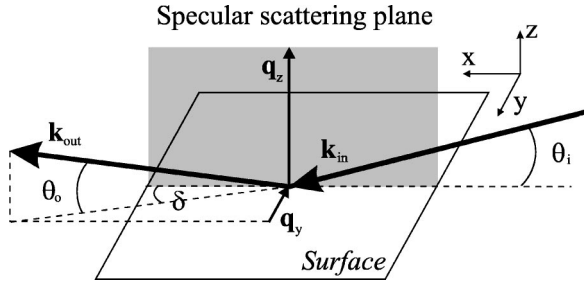*Corresponding author, email address: amadsen@esrf.fr

FIG. 1. Sketch of the scattering geometry for liquid samples.

specular reflected signal with momentum transfer $q_z = (4\pi/\lambda)\sin\theta_i$ perpendicular to the surface, could now be measured over a broad range of angles θ_i with $\theta_i = \theta_o$.

In GISAXS geometry [11,12], θ_i was kept at a value smaller than the critical angle α_c for total external reflection. The intensity could now be measured by scanning a vertical position-sensitive detector (PSD) horizontally (δ scan) to record the full scattering image. The PSD was placed so that the center channel corresponded to the specular position with $\theta_o = \theta_i = 0.1°$. In a δ scan, the momentum transfer has a component parallel to the surface given by $q_y = (2\pi/\lambda)\cos\theta_o\sin\delta$.

III. EXPERIMENTAL RESULTS

A. X-ray reflectivity

Specular reflectivity measurements ($\delta = 0, \theta_i = \theta_o$) were performed on two different colloidal samples, a concentrated suspension (40% wt.), a dilute suspension (1.8% wt.), and for reference on the solvent (water) only. The reflectivity profile for the pure water surface is indistinguishable from the one of the dilute sample as shown in Fig. 2. The profile from the concentrated sample, is however, strikingly different. The Fresnel reflectivity of an ideally sharp interface may be written as
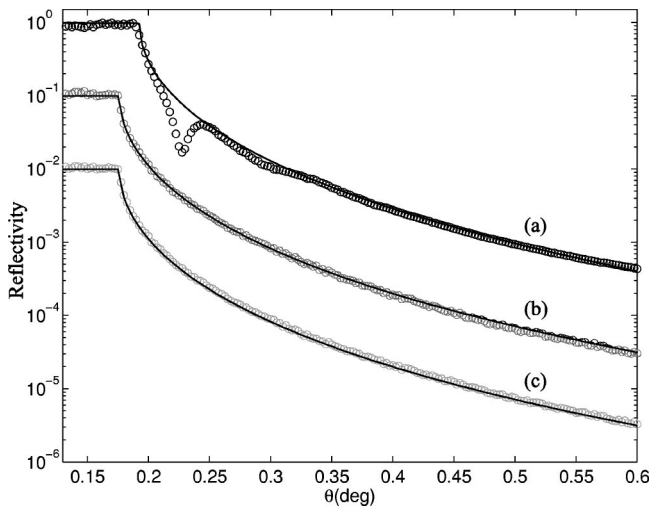

FIG. 2. Open symbols: Specular x-ray reflectivity profiles from the concentrated (40% wt.) colloidal suspension (a), the dilute (1.8% wt.), suspension (b), and pure water (c). The profiles (b) and (c) are offset by one and two decades, respectively. The solid lines are model fits to the data described in the text.

$$R_F = \left| \frac{\sin\theta_i - \sin\theta'}{\sin\theta_i + \sin\theta'} \right|^2, \qquad (1)$$

where θ' is the angle between the refracted beam and the surface. θ' is given by Snell's law $n\cos\theta' = \cos\theta_i$ where n is the refractive index of the sample. For x rays, we have $n = 1 - \delta$ with $\delta = \lambda^2 r_0 \rho^e/2\pi$ where r_0 is the Thomson scattering length of the free electron, ρ^e is the electron density of the sample, and λ is the wavelength. The Fresnel reflectivity has a critical angle $\alpha_c = \sqrt{2\delta}$ below which $R_F = 1$ and falls off asymptotically as q_z^{-4} (Porod's law) for large q_z. The solid line in Fig. 2(c) is a fit to the water data using the Fresnel reflectivity [Eq. (1)] multiplied by a Debye-Waller term $e^{-q_z^2\sigma^2}$ to account for the rms roughness σ of a water surface due to capillary waves. The fit yields $\rho^e/\rho_0^e = 1.005 \pm 0.023$ and $\sigma = 3.301$ Å ± 0.685 Å in good agreement with literature values for the electron density ($\rho_0^e = 0.334$ electrons/Å³) and the rms roughness of water [13]. An angular offset $\Delta\theta_i = 0.0225° \pm 0.0037°$ is introduced by the diffractometer line up. The reflectivity profile of the dilute suspension may also be described by the above-mentioned best fit to the water data as shown by the solid line in Fig. 2(b). Hence, the dilute suspension and pure water are indistinguishable in the reflectivity experiment.

The reflectivity profile of the concentrated suspension shown in Fig. 2(a) clearly differs from the other profiles (b) and (c). The larger critical angle reflects a larger electron density in this sample. The profile is furthermore modulated and shows a pronounced dip at $\theta \approx 0.23°$. The Fresnel reflectivity profile may be adjusted to match the larger critical angle but is otherwise clearly failing to describe the data as shown by the solid line in Fig. 2(a). The data around the dip fall significantly below this line indicating that a model based on Fresnel reflectivity plus additional small-angle scattering from the colloids would fail to fit the data [14]. Instead, we used Parratt's formalism [15,16], a recurrence formula where the reflecting medium is divided into slabs parallel to the surface, to calculate the reflectivity. The division into slabs (we use 300 slabs to cover a z range of 1500 Å) corresponds to a binning of $\rho^e(z)$ while the shape of $\rho^e(z)$ itself is determined by the model. A good fit to the data (solid line in Fig. 3) with a minimum of fit parameters is achieved by using three Gaussians centered at $z = 287, 626,$ and 918 Å with a full width at half maximum of about 275 Å and amplitude ratios of 4.0:2.6:1. The corresponding scattering length density (SLD) profile is illustrated in Fig. 4. The raise at the surface at $z = 0$ (not shown in Fig. 4) is described by an error function (derivative of Gaussian) with $\sigma = 3.301$ as previously found for pure water. We interpret this excess density along the surface normal direction as being due to a layering of the colloidal particles. The order is most pronounced near the surface and decreases rapidly so that only three layers may be clearly identified. Layering near a free surface has previously been observed with x rays for a thermotropic liquid crystal [17] and for liquid metals [18]. Layering of liquids near a solid interface has also been investigated with x rays [19]. We note that the small bump
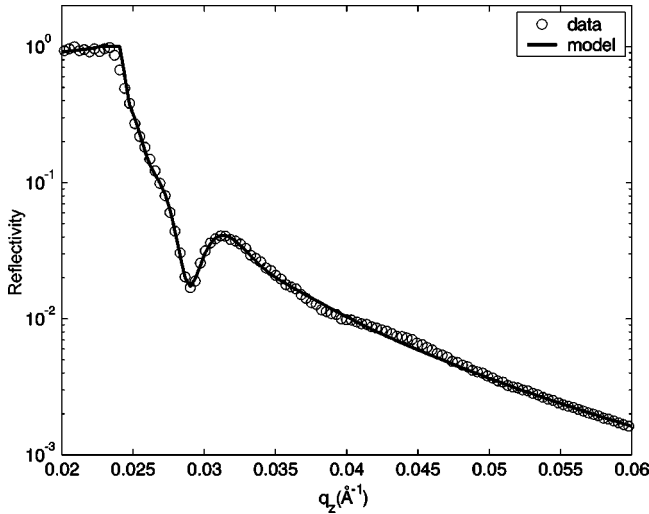
FIG. 3. Specular x-ray reflectivity profile from the concentrated (40% wt.) suspension compared to a model calculation (solid line) described in the text.

centered at $q_z = 0.045$ Å^{-1} in Fig. 3 is not reproduced. This reflects in our opinion the limitations of the applied model based on Gaussian profiles. The scattering length density for large z relaxes to a bulk level which is 22% bigger than the one of water (Fig. 4). This is consistent with the nominal weight concentration (40%) of silica colloids in the suspension if $\rho_c / \rho_0 = 1.82$ where ρ_0 and ρ_c are the mass densities of water and silica, respectively [20], although the value for ρ_c is somewhat lower than expected for pure silica. From the above-determined value of ρ_c, one may estimate the volume concentration of colloids to be about 27%.

Since only the averaged electron density of the sample along z is probed in a specular reflectivity experiment, it is not possible to draw conclusions about the shape and size of a particle. This information is however accessible by small-angle x-ray scattering (SAXS).
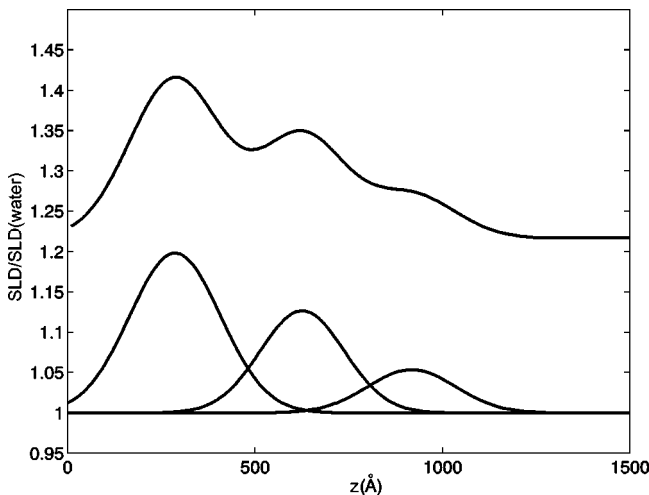

FIG. 4. The scattering length density z profile used in the model calculation to describe the data in Fig. 3. The profile consists of three Gaussians as shown in the lower part of the figure.
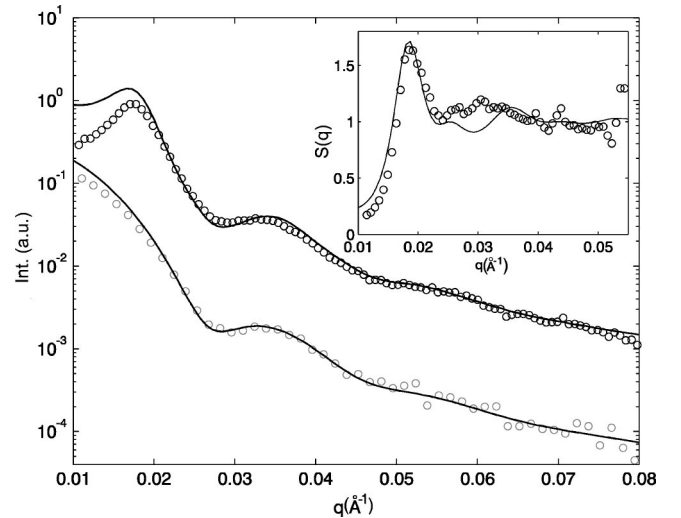

FIG. 5. SAXS profiles (open symbols) from the concentrated (top) and dilute suspension (bottom). Solid lines: Models as described in the text. Inset: $S(q)$ extracted as described in the text compared to a model fit with $R_S = 175$ Å and 27% vol.

B. Small-angle x-ray scattering (SAXS)

Both the concentrated and dilute samples were characterized by small-angle x-ray scattering. The corresponding SAXS profiles are shown in Fig. 5. The scattering intensity from a suspension of colloidal particles may be written as

$$I(q) \propto r_0^2 n_p (\rho_c - \rho_s)^2 V^2 F(q) S(q), \qquad (2)$$

where r_0 is the Thomson scattering length, n_p is the number density of particles, V is the particle volume and ρ_c, ρ_s are the electronic densities of the colloid and the solvent, respectively. $F(q)$ denotes the single-particle form factor of a homogeneous sphere with radius R_F given by [21,22]

$$F(q) = \left| \frac{\sin(qR_F) - qR_F \cos(qR_F)}{(qR_F)^3} \right|^2 \qquad (3)$$

and $S(q)$ is the static structure factor describing interparticle correlations. Size polydispersity may be taken into account by convoluting Eq. (2) with a size distribution function. The solid line in Fig. 5 (bottom) is a fit of Eq. (2) to the data taken on the dilute sample. The agreement at large q [$S(q) = 1$] is excellent and yields a sphere radius of $R_F = 161$ Å and a size polydispersity of 13% using the Schultz distribution [23]. The deviations from the model at low q indicate the presence of residual interactions with repulsive character [$S(q \to 0) < 1$]. A SAXS profile taken on the concentrated sample is shown in Fig. 5 (top). In contrast to the dilute sample, there is a pronounced maximum at low q indicating that strong interparticle interactions are present in the sample. The corresponding static structure factor was extracted by dividing the data from the concentrated sample by the form-factor $F(q)$ determined by fitting the high-q part of the dilute data (solid line in Fig. 5, bottom). The result is shown in the inset of Fig. 5. The static structure factor peaks at $qR_S \approx \pi$ where $2R_S$ is the center-to-center distance be-

tween two particles. The observed structure factor $S(q)$ may be approximately described in terms of an effective hard-sphere model. The repulsive interactions of the particles are taken into account by introducing an effective hard-sphere radius $R_S > R_F$ and an effective volume fraction into the Percus-Yevick approximation for hard spheres [24–26]. The result of such a fit to the data with $R_S = 175$ Å is also shown in the inset of Fig. 5 by the solid line. The model included a size polydispersity of 13% as found in the dilute case. Remarkably, the volume fraction of colloids is found to be 27.0% in good agreement with the value found in the XR experiment. The SAXS measurement clearly shows that the colloidal particles are neither aggregated nor do we see any sign of colloidal crystal formation or any particle sedimentation with time.

C. Grazing incidence small-angle scattering (GISAXS)

A measurement of the lateral organization of colloids near the surface is possible with the GISAXS technique. GISAXS measures small-angle scattering of the refracted beam. If the x-ray beam is incident below the critical angle $\alpha_c = \sqrt{2\delta}$, the small $1/e$ penetration depth Λ of the refracted evanescent wave

$$\Lambda = \frac{\lambda}{4\pi \, \mathrm{Im}\{\theta'\}} \simeq \frac{\lambda}{4\pi\alpha_c} \qquad (4)$$

ensures that the scattering is solely coming from the near surface region of the sample ($\Lambda \approx 50$ Å for pure water). Here, an incidence angle of 0.1° was used which is significantly below α_c for both the dilute and concentrated sample (see Fig. 2). Along the q_y direction (see Fig. 1), the scattering profile from an ideal liquid surface covered by capillary waves follows a power-law falloff due to the quasi-long-range correlations in the surface height [27]. Any deviation from this behavior here indicates the presence of small-angle scattering from colloidal particles. Hence, similar to a conventional SAXS experiment, a "GISAXS structure factor" was derived from the ratio between the two GISAXS profiles obtained on a concentrated and a dilute sample. The GISAXS profiles are extracted from the full-scattering image recorded with a vertical position-sensitive detector (PSD) by summing 10 channels (corresponding to $\Delta\theta_o = 0.01°$) about the center channel (corresponding to $\theta_o = 0.1°$). The results are shown as a function of q_y in Fig. 6. The double logarithmic plot emphasizes one major difference between the two curves: a different asymptotic power-law decay with q_y. In the dilute case, the curve (Fig. 6, upper curve) falls off as q_y^{-2}. The solid line is the calculated diffuse scattering profile from pure water [27]. It describes the overall decay of the experimental data very well and the deviations from the q_y^{-2} fall off are taken as being due to small-angle scattering from the colloids. The observed modulation might thus be interpreted as a "GISAXS form factor." The observation of particle scattering in the dilute case emphasizes one major difference between the GISAXS and XR techniques: The pure water and the dilute sample cannot be distinguished with the XR technique (Fig. 2), in contrast to the GISAXS technique
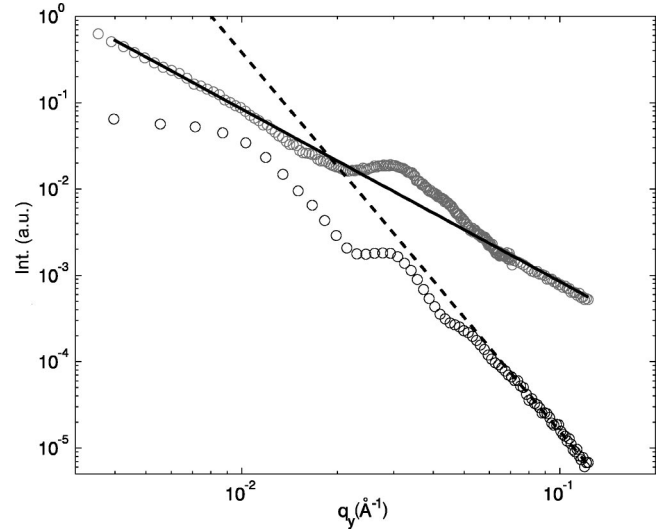

FIG. 6. GISAXS data from the dilute (upper curve) and the concentrated sample (lower curve). The concentrated data has been offset by one decade for clarity. The solid lines illustrates the asymptotic decays q_y^{-2} (dilute) and $q_y^{-4.39}$ (concentrated).

(Fig. 6) where they clearly can. The experiment on the concentrated sample (Fig. 6, lower curve) yields a GISAXS profile that falls off faster than q_y^{-4}. This is equivalent to what is observed when a graded density profile $\rho^e(z)$ is applied to describe the roughness of an otherwise ideally flat surface as previously discussed in the case of XR. The intensity becomes proportional to the product of the q^{-4} factor from Porod's law and the form factor of the graded interface that makes the intensity falloff faster than q^{-4} for high q. Here, this observation indicates that the surface colloids are randomly oriented since other surface morphologies would give different power-law behaviors [11,27,28]. This excludes, in particular, that the particles at the surface form a fractallike mesostructure or an ordered lateral structure as previously observed for floating colloidal particles at the air/water interface. The low q part ($q_y < 2 \times 10^{-2}$ Å^{-1}) of Fig. 6 behaves differently for the two profiles. This is quantified by the ratio between the curves plotted in Fig. 7. The resulting profile is reminiscent of the structure factor $S(q)$ observed by SAXS and shown in the inset of Fig. 5. We denote it the "GISAXS structure factor." The peak in Fig. 7 is thus suggesting the existence of correlations between the colloidal particles. From the peak position, we estimate a particle center to center distance of 570 Å, i.e., much larger than the layer spacing found from XR and the bulk-particle spacing $2R_S$ found by SAXS. The width of the peak in Fig. 7 indicates a correlation length of about 570 Å equal to the interparticle distance. Thus, the correlations range no longer than the distance between two particles. This is in agreement with the previous statement that the lateral arrangement of colloids at the surface is random.

IV. DISCUSSION AND CONCLUSION

X-ray reflectivity data were taken on three samples, a colloidal silica suspension (27% vol.), a dilute sample
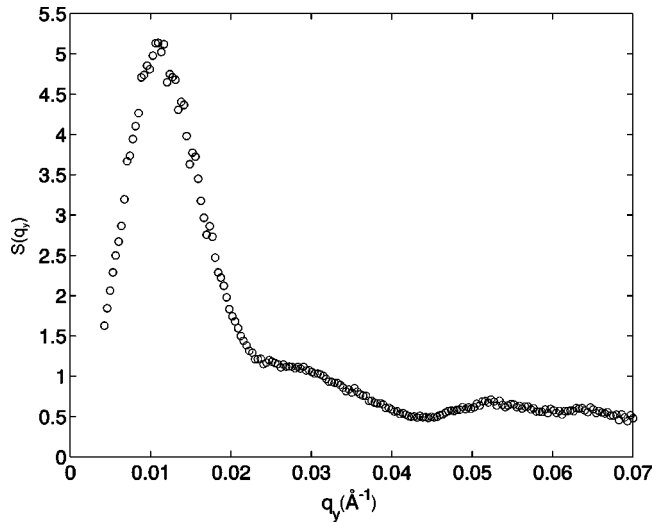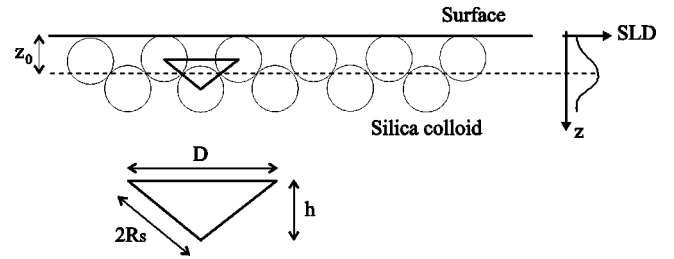
FIG. 7. Ratio between the GISAXS profiles from Fig. 6.

FIG. 8. Model of the organization of colloids near the surface. Note that the particles are just touching the surface with the perimeter.

(1.0% vol.), and pure water. The profiles clearly demonstrate that only the scattering length density along the surface normal (averaged over the footprint) influences the reflectivity. As a consequence, the form-factor oscillations of colloidal spheres do not show up in the XR intensity profile and the data for pure water and for the dilute sample are indistinguishable. XR measurements on the concentrated sample indicate that a particle layering near the free surface is occurring with the first layer being centered about 287 Å below the surface. To measure particle correlations at the surface GISAXS was used. The small penetration depth of grazing incidence x rays ensures us that only the first layer of colloidal particles is probed. For the dilute sample (1% vol.), a model for pure water describes the asymptotic behavior of the GISAXS profile well. In addition, a form-factor signal is present in the scattering profile. The GISAXS profile from the concentrated sample indicates that the lateral organization of colloids at the surface is random. The ratio of the GISAXS curves in Fig. 7 shows a broad peak at q_y $=0.01$ Å^{-1} that we assign to interparticle correlations. It is evident that the surface interparticle distance is larger along q_y (570 Å, Fig. 7) than along q_z (287 Å, Fig. 4) and that the interparticle distance found from the bulk-structure factor $S(q)$ (350 Å, Fig. 5, inset) is in between. A simple model for the arrangement of colloidal particles in the first few layers can be constructed as sketched in Fig. 8. If we use the parameters $D=570$ Å and $2R_S=350$ Å found from

GISAXS and SAXS, respectively, we find for the distance z_0 (see Fig. 8)

$$z_0 = R_S + \frac{h}{2} = R_S + \frac{1}{2}\sqrt{4R_S^2 - D^2/4} = 277 \text{ Å}. \qquad (5)$$

This is very close to 287 Å which was found to be the distance from the surface to the center of the first Gaussian in Fig. 4. Thus, in this picture, the Gaussians in Fig. 4 are just reflecting the excess scattering length density (SLD) due to the overlapping of layers of spheres along z when averaged in the x and y direction. The amplitude of the Gaussians gets smaller with increasing distance from the surface and three layers may be identified from XR. This indicates a transition from a bulk region to a near-surface region where the structure tends to display layering parallel to the surface. According to the above estimates, Fig. 8 would suggest that the colloids closest to the surface are just touching the water/vapor interface with their perimeter [29]. Thus, no increase in surface roughness due to the presence of colloidal particles is expected. This is in good agreement with the observation that the rms roughness of the surface (found from the XR measurements, see Fig. 2) is the same for the colloidal suspension and pure water. We might speculate that the weakly charged character of the particles together with the fact that they are still completely surrounded by water is in fact the reason why these colloids are not forming lateral surface structures contrary to what was previously observed for floating particles.

[1] P. Pieranski, Phys. Rev. Lett. **45**, 569 (1980).

[2] G. Y. Onoda, Phys. Rev. Lett. **55**, 226 (1985).

[3] R. Kesavamoorthy, C. Babu Rao, and B. Raj, J. Phys.: Condens. Matter **5**, 8805 (1993).

[4] A. E. Larsen and D. G. Grier, Nature (London) **385**, 230 (1997); W. R. Bowen and A. O. Sharif, *ibid.* **393**, 663 (1998).

[5] K. Zahn, R. Lenke, and G. Maret, Phys. Rev. Lett. **82**, 2721 (1999).

[6] D. Stamou, C. Duschl, and D. Johannsmann, Phys. Rev. E **62**, 5263 (2000).

[7] J. Stankiewicz, M. A. C. Vilchec, and R. H. Alvarez, Phys. Rev. E **47**, 2663 (1993).

[8] F. Ghezzi and J. C. Earnshaw, J. Phys.: Condens. Matter **9**, L517 (1997).

[9] The sample (Bindzil 40/130) was kindly donated by EKA Chemicals, Bohus (Sweden).

[10] J. Als-Nielsen, F. Christensen, and P. S. Pershan, Phys. Rev. Lett. **48**, 1107 (1982).

[11] J. R. Levine, J. B. Cohen, and Y. W. Chung, P. Georgopoulos, J. Appl. Crystallogr. **22**, 528 (1989); J. R. Levine, J. B. Cohen, and Y. W. Chung, Surf. Sci. **248**, 215 (1991).

[12] A. Naudon, T. Slimani, and P. Goudeau, J. Appl. Crystallogr. **24**, 501 (1991).

[13] A. Braslau, M. Deutsch, P. S. Pershan, A. H. Weiss, and J. Als-Nielsen, Phys. Rev. Lett. **54**, 114 (1985); A. Braslau, P. S. Pershan, G. Swislow, B. M. Ocko, and J. Als-Nielsen, Phys. Rev. A **38**, 2457 (1988).

[14] M. Maaza, A. Gibaud, C. Sella, B. Pardo, F. Dunsteter, J. Corno, F. Bridou, G. Vignaud, A. Desert, and A. Menelle, Eur. Phys. J. B **7**, 339 (1999).

[15] L. G. Parratt, Phys. Rev. **95**, 359 (1954).

[16] X.-L. Zhou and L. He, Phys. Rev. E **49**, 5345 (1994).

[17] B. M. Ocko, A. Braslau, P. S. Pershan, J. Als-Nielsen, and M. Deutsch, Phys. Rev. Lett. **57**, 94 (1986).

[18] O. M. Magnussen, B. M. Ocko, M. J. Regan, K. Penanen, P. S. Pershan, and M. Deutsch, Phys. Rev. Lett. **74**, 4444 (1995); M. J. Regan, E. H. Kawamoto, S. Lee, P. S. Pershan, N. Maskil, M. Deutsch, O. M. Magnussen, B. M. Ocko, and L. E. Berman, *ibid.* **75**, 2498 (1995).

[19] W. J. Huismann, J. F. Peters, M. J. Zwanenburg, S. A. de Vries, T. E. Derry, D. L. Abernathy, and J. F. van der Veen, Nature (London) **390**, 379 (1997); A. K. Doerr, M. Tolan, T. Seydel, and W. Press, Physica B **248**, 263 (1998); C.-J. Yu, A. G. Richter, J. Kmetko, S. W. Dugan, A. Datta, and P. Dutta, Phys. Rev. E **63**, 021205 (2001).

[20] Here, we moreover assume that $\rho_c^e/\rho_0^e = \rho_c/\rho_0$. We estimate this to cause a maximum error of 10% unfortunately inevitable since the exact chemical composition of the colloids is unknown.

[21] A. Guinier and G. Fournet, in *Small Angle Scattering of X-rays* (Wiley, New York, 1955)

[22] H. Brumberger, in *Modern Aspects of Small Angle Scattering* Vol. 451 of *NATO Advanced Studies Institute, Series C*, edited by H. Brumberger (Kluwer Academic Press, Dordrecht, 1993).

[23] M. Kotlarchyk and S. Chen, J. Chem. Phys. **79**, 2461 (1983).

[24] J. K. Percus and G. J. Yevick, Phys. Rev. **110**, 1 (1958).

[25] N. W. Ashcroft and J. Lekner, Phys. Rev. **145**, 83 (1966).

[26] J. P. Hansen and I. R. McDonald; *Theory of Simple Liquids* (Academic Press, New York, 1986).

[27] S. K. Sinha, E. B. Sirota, S. Garoff, and H. B. Stanley, Phys. Rev. B **38**, 2297 (1988).

[28] H. D. Bale and P. W. Schmidt, Phys. Rev. Lett. **53**, 596 (1984).

[29] The discrepancy between z_0 (277 Å) and the distance from the surface to the center of the first Gaussian (287 Å, see Fig. 4) actually suggests that on average the colloids are located 10 Å below the surface.